

A Dual Stream Spectrum Deconvolution Neural Network

Lizhen Deng, *Member, IEEE*, Guoxia Xu, *Member, IEEE*, Yanyu Dai, and Hu Zhu, *Member, IEEE*,

Abstract—With the development of spectral detection and photoelectric imaging, multi-band spectrum is always degraded by the random noise and band overlap during the acquisition of spectrum devices. Owing to the fixed spectrum degradation model, the existing spectrum deconvolution technologies are sensitive to the handcrafted model designed and manually selected parameters. The fundamental cause of these limitations during spectral analysis is that spectral processing is limited by one-dimensional signal without structural information available and insufficient training samples. In this paper, a dual stream neural network is proposed to reconstruct the original infrared spectroscopy, which effectively strengthens the capability to represent the feature of infrared spectrum. A novel activation function is proposed to realize the function of the dual stream network. Furthermore, a heuristic learning strategy from the perspective of balanced self-paced learning is exploited to help network train from simple to difficult, resolving the problem of high sample repeatability. Compared with other traditional methods, the experimental results show that our network can achieve state-of-the-art reconstruction result and fairly excellent performance in terms of the corresponding index within synthetic and real spectrum experiments.

Index Terms—Spectral Deconvolution, Industrial Spectrum, Dual Stream Network

I. INTRODUCTION

BASED on the great accuracy in distinguishing the chemical composition and molecular structure, spectrum is widely used in various areas, such as liquid detection [1], medicine testing [2], chemicals structure analysis [3], biological materials [4], medical image [5], food quality [6] and so on. However, in the process of obtaining the spectrum, the spectrum is often degraded by many objective factors: the tremble of spectrometer and natural random noise (so called the instrument broadening function (IBF)). The degraded spectrums make it difficult to get accurate information of structure and molecule. To handle with this problem, a large number of reconstruction algorithms have been proposed to recover the peak or valley and preserve the spectrum structure details. Recently, deconvolution method has received considerable critical attention in the field of signal recovery for long time. The core idea of the deconvolution method is to simulate the process of convolution to recover the degraded spectrum.

This work is supported by the National Natural Science Foundation of China under Grant 62072256. (Corresponding author: Hu Zhu) (E-mail: peter.hu.zhu@gmail.com)

Lizhen Deng is with National Engineering Research Center of Communication and Network Technology, Nanjing University of Posts and Telecommunications, Nanjing, 210003, China. Guoxia Xu is with Department of Computer Science, Norwegian University of Science and Technology, 2815 Gjøvik, Norway. Yanyu Dai and Hu Zhu are with Jiangsu Province Key Lab on Image Processing and Image Communication, Nanjing University of Posts and Telecommunications, Nanjing 210003, China.

In general, the existing deconvolution methods can be classified into non-blind deconvolution (NBD), blind deconvolution (BD) and semi-blind deconvolution (SBD). For NBD method, the Fourier self-deconvolution (FSD) [7] method is one of the simplest deconvolution techniques to process spectroscopic. According to these studies, maximum burg entropy deconvolution (MaxEntD) [8] method was proposed to resolve the spectral deconvolution problem. However, these methods mentioned above all rely on the prior knowledge of frequency domain information and spectral domain information. In the case of few available samples, the non-blind model relies too much on prior knowledge, which leads to overfitting and poor robust performance. In order to minimize the impact of this limitation, many SBD methods [9] [10] [11] based on various regularizations have been developed to solve problems such as over-fitting caused by excessive reliance on prior knowledge. However, the uncertain blur kernel will cause poor reconstruction results under non-gaussian like IBF assumption.

Recently, blind deconvolution methods became more and more popular in the field of deconvolution without fixed IBF in advance. The BD methods estimate the blur kernel and clean spectrum data simultaneously from the observation spectrum without any prior knowledge. Therefore, blind deconvolution (BD) [12], [13] [14][15] methods are considered to be a more reasonable method in practical applications. But the unknown IBF and latent spectral information make the learning process difficult. Generally speaking, all of the above methods have their own limitations more or less. These limitations are mainly reflected in: single processing mode, relying on prior knowledge, manually designing parameters, and high computational complexity for iterative optimization. Thus, our goal is to propose a spectrum deconvolution method regardless of any kind of IBF and noises.

In the last few years, with the rapid development of neural networks, the application of neural network has applied to various such filed. Some neural networks which used to image processing have been proposed, including stacked auto-encoder structure [16], convolutional neural network [17], fully convolutional network [18]. By summarizing the process of these networks, data-driven works enable the desirable behaviors in tailoring the task from the perspective of feature representation strategies and sample learning modes. Motivated by the scale-variant of network design, like Lin et al. [19] proposed feature pyramid network to object detection. This feature pyramid network (FPN) was designed to solve multi-scale problem in small object detection by concatenating the feature map of each resolution. Various of scale-variant methods dominates the feature representation strategies domain

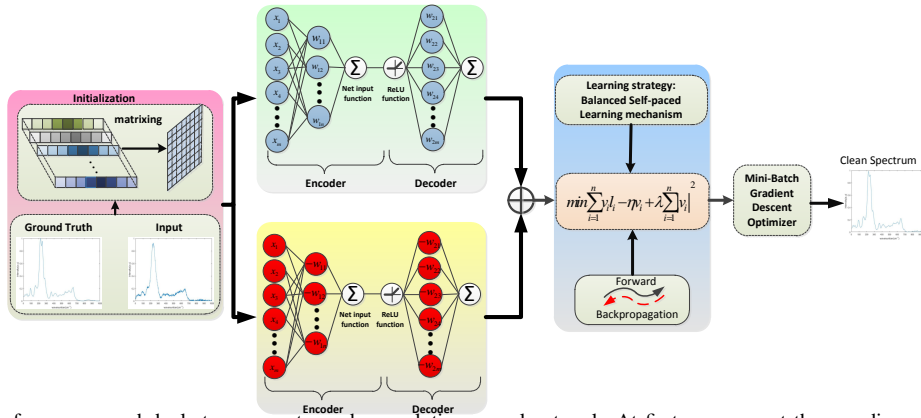


Fig. 1. The framework of our proposed dual stream spectrum deconvolution neural network. At first, we convert the one-dimensional spectrum into matrix and initialization. The input is redirected into stream A and stream B. the output is obtained by adding the result of two streams. Network structure of every stream is symmetric about the coding layer (the middle hidden layer). Therefore, the output spectrum and the input degraded infrared spectrum have the same length.

in general network design. Unfortunately, due to the one-dimensional continuity of different frequency bands for spectrum processing, scale-variant approach mentioned above is not optimal for infrared spectrum to extracting feature. In [20], they proposed a lightweight dilated convolution module to deal with the spectral deconvolution (SD) problem. Although this method has achieved superior performance to the recovery of infrared spectral signals, this dilated convolution module focuses on the local features of the spectrum. For the one-dimensional spectrum, global features of spectrum are more significant than local features. Thus, in this work, two new problems are mainly focused on from the perspective of data-driven manner: 1: *how to enrich sample features and sharp knowledge over spectrum*; 2: *how to solve sample problems through heuristic sample learning strategy in signal domain, such as self-paced learning* [21].

In this paper, in order to overcome the lack of prior knowledge and the complexity of manual design of model, the data-driven method is used. The data-driven method of spectral deconvolution eliminates the need for complex convolution theory, and only using data to train neural networks can surpass the effects of artificially designed network models. The main contributions in this paper are presented as follows:

- A symmetrical dual stream neural network stream is proposed to enhance feature extraction for spectrum, including peaks and flat areas. In order to simplify the network, a novel activation function is proposed to realize the function of the symmetrical dual stream network. It can ensure the effectiveness of feature extraction and make network having a faster processing speed than other convolution networks.
- A more reasonable learning strategy, balanced self-paced learning [22], is quoted into our objective loss function to resolve the problem of high sample repeatability.

II. MOTIVATION

With the rapid development of deep learning, many related methods have been proposed for various practical application scenarios. In [23], a bilinear CNN model is proposed to refine visual recognition. The network architecture consists of two

feature extractors. Each feature extractor can be viewed as a CNN whose output is multiplied by the output of each CNN. In this way, a recognition architecture is proposed, which is composed of two feature extractors. The output of these feature extractors is multiplied by an external product at each position of the image, and then combined to obtain an image descriptor. The differences in feature richness between the spectral signal and the image are taken into account. A dual stream network is proposed to extract spectral features and connect the output with each network stream. The architecture of each network stream is similar to auto-encoder [24]. Autoencoder is a kind of network that plays a vital role in deep learning. Several studies have shown its advantages in feature extraction and processing. Unlike the autoencoder network structure, the corresponding parameters of the network are trained in a supervised mode. Since our network extracts features separately from the low-frequency information and high-frequency information in the spectral signal, it greatly improves the ability of our model to pay attention to high- and low-frequency information. Each of the dual stream networks is regarded as a separate CNN, so it has a higher anti-interference ability against noise.

In terms of learning strategy, in [20], self-paced learning is used to accelerate the model convergence speed. In this work, considering the impact of sample repetition on the training process, this paper decided to adopt another similar learning strategy, self-paced learning to solve this problem.

III. OUR APPROACH TO SPECTRUM DECONVOLUTION

A. Network Architecture

The overall Framework of the network is shown in Fig.1. The basic structure of our network is similar to the auto-encoder. But different from auto-encoder, supervised feature representation is mainly considered in our work during training process. Our neural network consists of two parts: an encoder (recognition network) and a decoder (generative network). The encoder converts the input into a simpler, internal representation, and the decoder is responsible for producing the output from the internal representation. Note that the hidden layer must have less neuron in order to force the network to learn

the most important features in the data. That way, it cannot trivially copy the input to the output. Since the hidden layer has a lower dimensionality than the output, the auto-encoder is said to be under-complete. Just like other neural networks, this network can also have multiple hidden layers. More hidden layers will allow the network to learn more complex features. For spectrum signals, if too many hidden layers embedding in the designed network are likely to be overfitting for the training. Indeed, only this single architecture may be difficult in learning a latent representation from the training samples directly.

Hence, the inversed stream that mentioned in the neural network architecture is added to settle this limitation. The inversed stream is used to learn the corresponding clean atoms by detecting inversed blurry input patterns. The basic ideal of inverse stream is that for the same hidden layer, another neural nodes are introduced, which receive opposite input and output weights to model two-factor variations for spectrum. Hence, this model can extract the corresponding information for spectrum more efficient. According to the activation function in hidden layer, instead of using tanh or sigmoid, rectified linear unit (ReLU) is proved to handle vanishing gradient problem. Next, a novel activation function will be proposed which can realize this inversed stream architecture.

Considering the complexity of the derivation process, this activation function is introduced based on a hidden layer network structure. As shown in Fig.2. The ability of our neural network to extract the high and low frequency features of the infrared spectrum can be shown clearly in the figures. In this way, the forward propagation can be described as follows:

$$Y = [W_2 - W_2] h \left(\begin{bmatrix} W_1 \\ -W_1 \end{bmatrix} \tilde{X} + \begin{bmatrix} b_1^u \\ b_1^l \end{bmatrix} \right) + b_2 \quad (1)$$

where \tilde{X} is the input, Y is the corresponding output from the last layer. And $W_1, W_2, b_1^u, b_1^l, b_2$ denote the matrix parameters that need to be learned in network, in which b_1^u, b_1^l represent the bias that corresponding to the upper stream and lower stream in hidden layer respectively. $h(x)$ is the rectified linear unit (ReLU) $\max(0, x)$. According the above formulation, a novel function is proposed with a trainable parameter t to combine these two streams into one unified framework:

$$g(x) = \max(0, x + t) - \max(0, -x + t) \quad (2)$$

Let $t = (b_1^u + b_1^l)/2$. Then, the forward propagation can be transformed as follows:

$$Y = W_2 g \left(W_1 X + \frac{b_1^u - b_1^l}{2} \right) + b_2 \quad (3)$$

According to the above derivation process, this function is depicted with different parameter t in Fig.3. During the training process, all of the parameters in the process of forward propagation can be learned by using back-propagation algorithm, minimizing the empirical squared error between obtained degraded infrared spectrometers and the corresponding label. The partial derivative of $g(x)$ with respect to t can be written as follows:

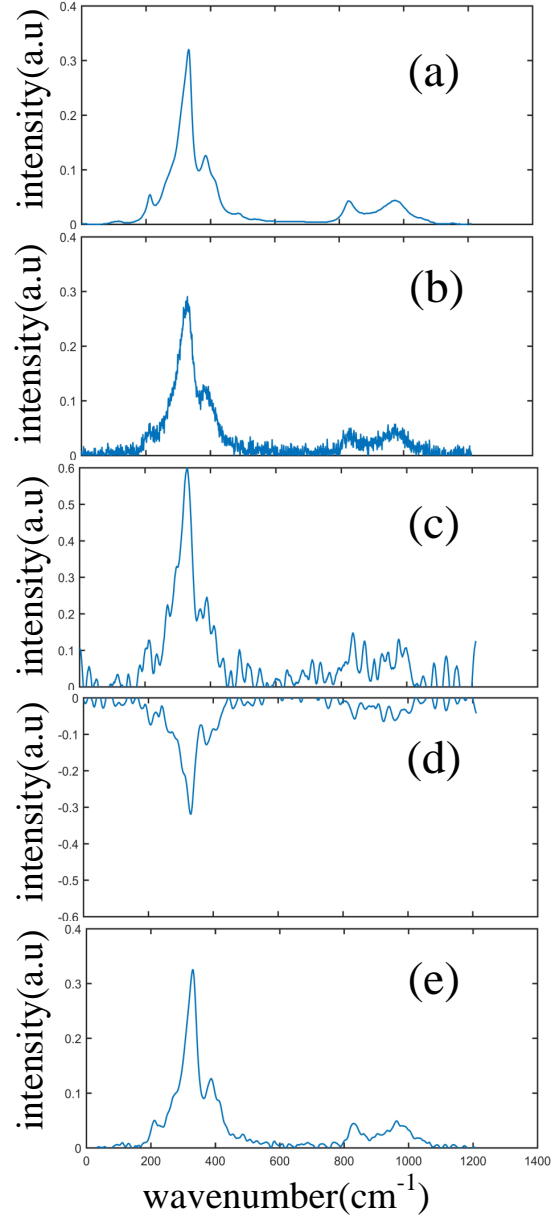


Fig. 2. Understanding the architecture of the dual stream neural network with hidden layers. (a). The original infrared spectrum. (b). The degraded infrared spectrum under noisy condition. (c). The corresponding high frequency of the infrared spectrum extracted by the stream A neural network. (d). The corresponding low frequency of the infrared spectrum extracted by the stream B neural network. (e). The output of the neural network

$$\frac{\partial g(x)}{\partial t} = \begin{cases} 0 & x \leq |t| \\ \text{sgn}(x) & x > |t| \end{cases} \quad (4)$$

Compared with using two rectified linear units (ReLU), this novel activation function reduces the number of model parameters by a large factor while preserving the architecture of inverse stream and simplifies the gradients in the training process. It not only has the advantages of ReLU activation function: nonlinear, easy to derive, but also shortens the training steps: A unified network with a novel activation function can be used instead of a dual stream neural network to share neuron weights and reduce the number of forward

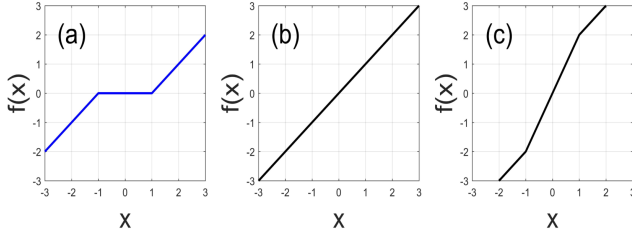


Fig. 3. Activation function with the parameter t , (a). t is nonnegative ($t=1$). (b). t is zero ($t=0$). (c). t is negative ($t=-1$).

and back propagation, making the dual stream network more compact and more integrated, rather than two separate parts.

B. Objective Loss Function with Balanced Self-paced Learning

Inspired by above theory of self-paced learning, the key principle of self-paced learning is used to optimize the objective function. This improvement could help our model become more comprehensively to solve spectrum deconvolution problem. Formally, given an output of the network $f(x_i, w)$, w represents all the parameters in our network. x_i, y_i denotes the i^{th} degraded spectrum and ground truth in the training process. N is the number of training sample in data set. Therefore, the loss function can be formulated as follows:

$$L(y_i, f(x_i, w)) = \frac{1}{2N} \sum_{i=1}^n (y_i - f(x_i, w))^2 \quad (5)$$

Obviously, the loss function is the mean-square error (MSE). In order to represent briefly, letting $l_i = L(y_i, f(x_i, w))$ in the following section. Based on the loss function and the methodology of standard self-paced learning (SPL), the objective function is reconstructed by adding a hard self-paced regularization term and weighted loss function term into the loss function. The objective loss function can be written as:

$$E(w, v; \eta) = \arg \min \sum_{i=1}^n v_i l_i - \eta v_i \quad (6)$$

In this objective function, as mentioned in above section, the parameter η is a threshold (age parameter) that controls the learning pace. At the same time, the difference of sample can be got by computing the mean-square error (MSE) of samples. The value of η is the latent weight variable in the self-paced learning (SPL), which decide whether the input samples can be selected or not. If $l_i < \eta$, the self-paced learning parameter is $v_i = 1$, otherwise $v_i = 0$. While this improvement could help the model dynamically build a robust self-paced learning (SPL) system, there is an issue existing in the process of training. The self-paced learning (SPL) could be seen as selector that get easier samples. That is to say, the neural network may select only a few easier samples repeatedly under the influence of self-paced learning. To handle this limitation, a penalty term is added into the objective function that balances the lack of sample diversity, named balanced

self-paced learning (BSPL) [22]. Intentionally, the objective loss function can be transformed as follow:

$$E(w, v; \eta, \lambda) = \arg \min \sum_{i=1}^n v_i l_i - \eta v_i + \lambda \sum_{i=1}^n |v_i|^2 \quad (7)$$

where λ is the hyper-parameter, the component of the balanced self-paced learning objective loss function can be divided into two regularization terms. The first term is responsible for selecting easier samples and the second term penalizes the training samples with more selected. Thus, the proposed objective function considers both the easiness and diversity of selected samples to remove redundant information and accelerate training steps. Based on the objective loss function, the global optimum solution for this optimization problem can be derived as follows:

$$v_i = \begin{cases} 0, & l_i \geq \eta - 2\lambda(q-1) \\ \eta - l_i/2\lambda, & \eta - 2\lambda q \leq l_i < \eta - 2\lambda(q-1) \\ 1, & l_i < \eta - 2\lambda q \end{cases} \quad (8)$$

$q \in \{1, \dots, n\}$ is the sorted index based on the loss values $\{l_1, \dots, l_n\}$ in the k^{th} training sample. This formula can intuitively explain the advantages of this optimization, which can classify samples according to the size of the sample loss. If the loss of training sample is less or greater than the threshold $\eta - 2\lambda q / \eta - 2\lambda(q-1)$, the sample would be considered as easy or difficult sample and are selected or not selected into the neural network. Otherwise, the sample would be considered as medium condition that is between easy and difficult.

C. Training of Neural Network

The manually degraded infrared spectral data sets are put into training in our work. Based on the methodology of degraded spectrum model, the process of spectral degradation is simulated by appending different blur kernels, such as Gaussian blur and Lorentz blur, to the clean infrared spectrum; the original clean infrared spectra are gained from high precision infrared spectrometer. The specific scheme of updating parameter is illustrated in Fig.4. In order to get the global optimal solution, Mini-Batch Gradient Descent (MBGD) is used to update the parameter. Hence, all the training samples are divided into many batches; every batch contains several degraded spectrums. Meanwhile, the BatchNormalization (BN) aims to solve the inefficient training. It normalizes the statistical distribution of all samples to reduce the difference between different samples in the batch. Therefore, BatchNormalization (BN) allows to use a large learning rate for training during the training process.

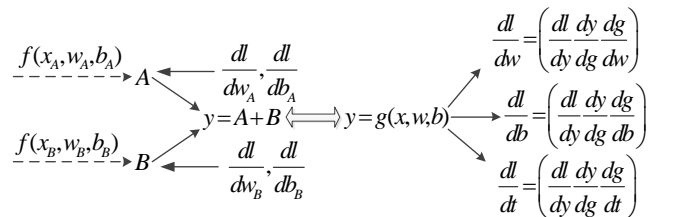


Fig. 4. Computing the gradients of dual stream network in the model and transform it into a more concise solution.

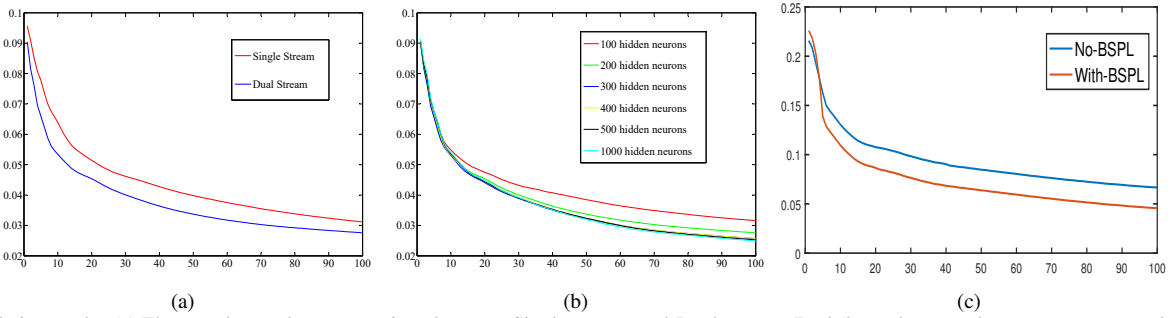


Fig. 5. Ablation study: (a).The test dataset loss comparison between Single stream and Dual stream (Both have the same hyper parameters and the number of neurons) during the training process. (b).The test dataset loss comparison on different numbers of neurons during the training process. (c).Comparison between No-BSPL (Our method without Balanced Self-Paced Learning) and With-BSPL (Our method with Balanced Self-Paced Learning during the training process).

Algorithm 1 The optimization of our method

- Step 1. Initialize the parameters of network, age parameter η and weight factor v .
 - Step 2. Carrying out the forward propagation and calculate the loss function of training samples.
 - Step 3. Decide whether the sample can be selected by comparing loss function with age parameter η .
 - Step 4. If selected, update the parameter by Mini-Batch Gradient Descent (MBGD), else, reselect the training sample to repeat step2 until the v is not equal to 0.
 - Step 5. Update $\eta = k\eta, k > 1$.
 - Step 6. Repeat step2 to step5 until the test samples can converge to a certain value of root mean square error (RMSE), and then save the corresponding parameters.
-

According to the iterating algorithm, alternative learning approach is used to update the parameters, hence, the process of updating parameter (w, v) can be divided into two parts: 1) If the w is fixed, the self-paced learning parameter v can be determined by comparing the loss function of train sample with age parameter η , that is say, the train sample would be labeled or unlabeled. 2) Based on the label train samples and fixed parameter v , all the network parameters (w) including weights (W_1, W_2), biases (b_1^u, b_1^l, b_2), extra parameter (t) would be learned by back propagation algorithm. Network training follows the basic principle of gradient descent, because the derivatives of each activation function exist, as long as the learning rate is controlled, the convergence of the network can be guaranteed.

Based on these theories, the optimization of our proposed method can be formulated as algorithm 1.

IV. EXPERIMENTAL RESULTS AND DISCUSSION

A. Experimental Settings

Our proposed method is based on deep learning neural network training, in which the parameters involved have weight value w , bias b , and additional parameter t . In order to avoid the impact of overfitting on the model but also to ensure the accuracy of the model, the number of neural network nodes trained in the model is 300. Because there is no unified dataset, the dataset used in our work contains 24696 pieces of

spectral data from the Internet and from our own collection. The wavenumber of each spectral data is 1211. In order to imitate the situation under different noises, degraded spectral data are generated by adding different kinds of noise. During the training process, the mini batch size and learning rate is set to 256 and 0.00001. Parameter initialization obeys normal distribution. Our methods is implemented with Matlab 2017a and all the experiments are run on a PC equipped with Intel i7 7700 CPU, 32GB RAM and a single NVIDIA GTX 1070 GPU. Several deconvolution methods for spectral resolution enhancement, SBD-MHS [25], SBD-HS [26], MaxEntD [8], DSPNet [20] are chosen for comparison with the proposed method. The training of all models follow the criteria of the original papers. To compare the performance of our method with other methods quantitatively, there are several indexes to evaluate the reconstructed spectral quality: root mean square error (RMSE), weighted correlation coefficient (WCC), and correlation coefficient (CC). For RMSE, WCC and CC (The details can be found in [20]), the range of them is zero to one.

B. Ablation Study

In order to compare the performance between single stream and dual stream, a single stream network is designed with the same hidden nodes of dual stream network. The comparison of results are shown in Fig.5(a), the performance of our proposed dual stream structure is shown clearly. The loss of dual stream is always lower than that of single stream, it proves that the dual stream network can extract more useful features and have a better and faster performance.

In order to compare the performance of network with different numbers of hidden neurons, the experiments with same training process and different numbers of hidden neurons are designed. The results are shown in Fig.5(b). The picture shows that when the number of hidden neurons exceeds 300, there is little change between network losses. In order to reduce the phenomenon of network overfitting, but also to speed up the network speed and ensure the accuracy of the network, 300 is the most appropriate number of hidden neurons.

In the Fig.5(c), we compare the impact of balanced self-learning. It is evident that, at the beginning of learning state, our method has faster convergence rate. In general, the BSPL model accelerates the learning process and prevents the network falling into the local minimization value. This

improvement could help the model automatically adjust its course materials, establishing a sound BSPL system.

C. Deconvolution of Single Blur Kernel Spectrum

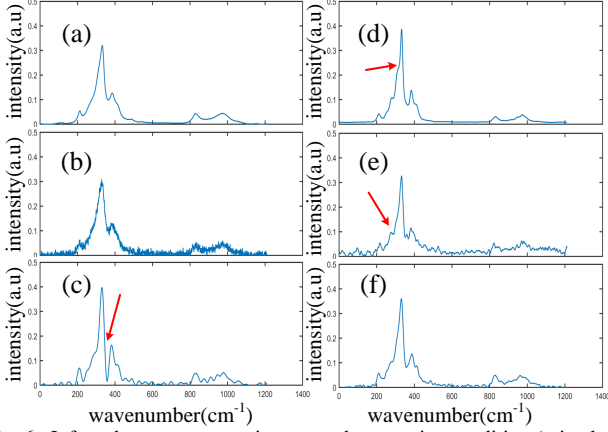


Fig. 6. Infrared spectrum experiments under no noisy condition (mixed mixed blur kernel: $\rho_{gauss} = 8$, (a) Original spectrum, (b) Degraded spectrum under noisy condition $var = 10$, (c) Recovery spectrum of SBD-HS , (d) Recovery spectrum of MaxEntD, (e) Recovery spectrum of DSPNet , (f) The results of our method

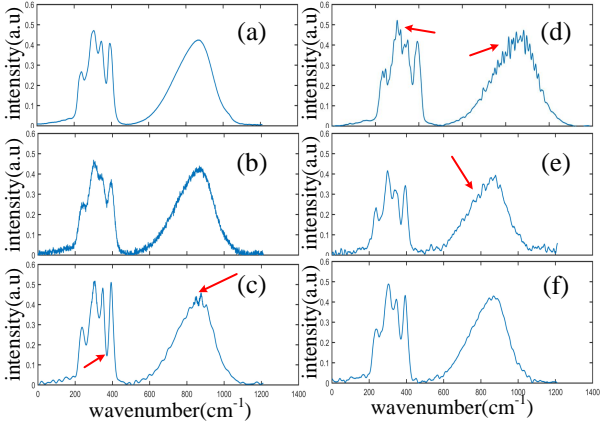


Fig. 7. Infrared spectrum experiments under noisy condition (mixed mixed blur kernel: $\rho_{gauss} = 7$, $\rho_{lorentz} = 7$, (a) Original spectrum, (b) Degraded spectrum under noisy condition, (c) recovery spectrum of SBD-MHS , (d) recovery spectrum of MaxEntD, (e) recovery spectrum of DSPNet , (f) the results of our method

TABLE I
AVERAGE PERFORMANCE COMPARISON UNDER MIXED KERNELS
($\rho_{gau} = 8$).

Noise level	Method	RMSE	CC	WCC
Noise- free	SBD-HS	0.0134	0.9610	0.9514
	SBD-MHS	0.0209	0.9217	0.9087
	MaxEntD	0.0094	0.9718	0.9713
	DSPNet	0.0211	0.9638	0.9718
	OurMethod	0.0066	0.9927	0.9916
$Var = 10$	SBD-HS	0.0136	0.9586	0.9518
	SBD-MHS	0.0214	0.9176	0.9053
	MaxEntD	0.0097	0.9786	0.9749
	DSPNet	0.0220	0.9629	0.9700
	OurMethod	0.0066	0.9927	0.9915

The deconvolution results of single blur kernel spectrum are illustrated in Fig.6 and Table. I. The Fig. 6(b) is the degraded

spectrum, involving with a Gaussian-shape instrument function $\rho_{gauss} = 8$ with a Gaussian noise $var = 10$. It can be seen in Fig. 6(c), the SBD-HS method restores the valley position well marked in Fig. 6(c). The DSPNet cannot remove noise well in the flat area of the spectral signal. Through the above experimental results and related indicators, our method gets better performance especially in the recovery of small details.

D. Deconvolution of Mixed Blur Kernel Spectrum

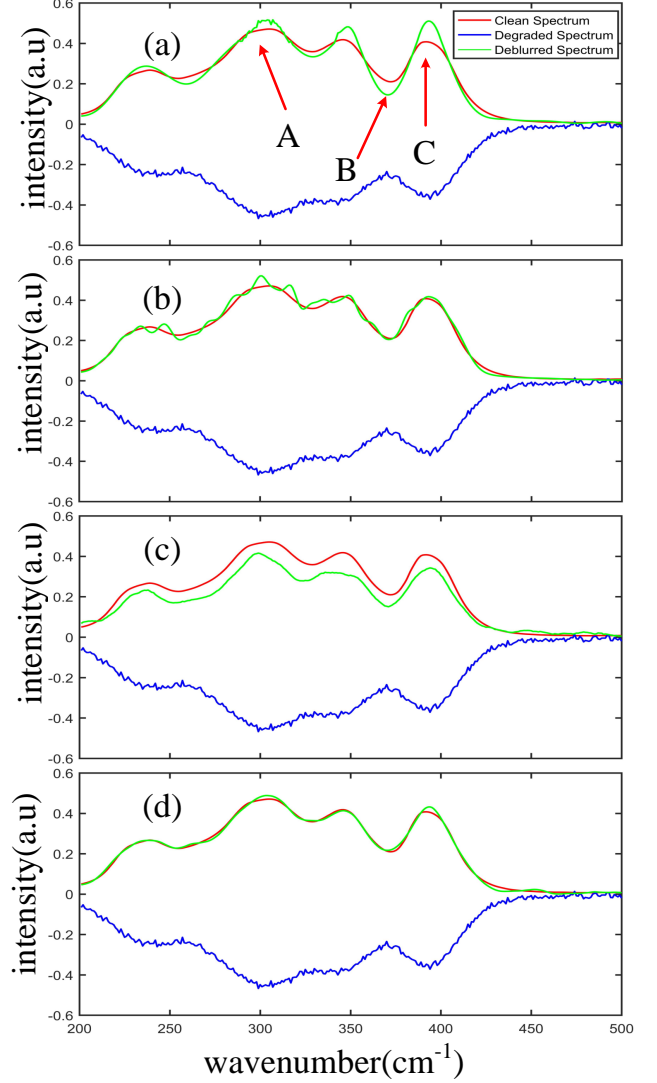


Fig. 8. The part of deconvolution results about Fig. 7 for different methods, the part of spectrum is from 200 cm^{-1} to 500 cm^{-1} The (a) SBD-MHS, (b)MaxEntD, (c) DSPNet, (d) OurMethod

In order to verify robustness of our method under complex situations. the mixed blur kernel experiments are proposed, whether additive Gaussian noise or no noise, to realize it. According to the spectral degraded model, the degraded spectrum is degraded spectrum by Gaussian and Lorentzian blur kernel together.

As indicated by the arrows in Fig.7 and Either SBD-MHS or MaxEntD, these two methods can not recover it well in the area of valley, for example, the SBD-MHS can not recovery the degraded area well as over-smooth and the

TABLE II
THE PERFORMANCE OF DIFFERENT METHODS UNDER VARIOUS SITUATION

Method	ρ_{Gau}	ρ_{Lor}	Noise level	RMSE	CC	WCC	
SBD-HS	5	6	Noise-free	0.0113	0.9662	0.9583	
			Var=0.01	0.0121	0.9607	0.9559	
	5	7	Noise-free	0.0119	0.9655	0.9564	
			Var=0.01	0.0125	0.9606	0.9552	
	6	6	Noise-free	0.0117	0.9651	0.9562	
			Var=0.01	0.0121	0.9625	0.9571	
	6	7	Noise-free	0.0117	0.9651	0.9562	
			Var=0.01	0.0121	0.9625	0.9571	
	7	5	Noise-free	0.0117	0.9651	0.9562	
			Var=0.01	0.0121	0.9625	0.9571	
	7	7	Noise-free	0.0117	0.9651	0.9562	
			Var=0.01	0.0121	0.9625	0.9571	
	SBD-MHS	5	6	Noise-free	0.0168	0.9426	0.9350
				Var=0.01	0.0170	0.9405	0.9332
5		7	Noise-free	0.0179	0.9375	0.9275	
			Var=0.01	0.0181	0.9343	0.9251	
6		6	Noise-free	0.0173	0.9406	0.9309	
			Var=0.01	0.0174	0.9375	0.9292	
6		7	Noise-free	0.0180	0.9366	0.9260	
			Var=0.01	0.0183	0.9346	0.9252	
7		5	Noise-free	0.0176	0.9375	0.9291	
			Var=0.01	0.0175	0.9366	0.9275	
7		7	Noise-free	0.0186	0.9338	0.9227	
			Var=0.01	0.0192	0.9306	0.9210	
MaxEntD		5	6	Noise-free	0.0088	0.9758	0.9722
				Var=0.01	0.0109	0.9801	0.9691
	5	7	Noise-free	0.0085	0.9763	0.9766	
			Var=0.01	0.0105	0.9801	0.9749	
	6	6	Noise-free	0.0086	0.9753	0.9717	
			Var=0.01	0.0103	0.9794	0.9705	
	6	7	Noise-free	0.0085	0.9762	0.9767	
			Var=0.01	0.0106	0.9797	0.9731	
	7	5	Noise-free	0.0083	0.9761	0.9750	
			Var=0.01	0.0098	0.9820	0.9751	
	7	7	Noise-free	0.0085	0.9753	0.9772	
			Var=0.01	0.0101	0.9814	0.9778	
	DSPNet	5	6	Noise-free	0.0203	0.9723	0.9811
				Var=0.01	0.0212	0.9714	0.9792
5		7	Noise-free	0.0203	0.9735	0.9821	
			Var=0.01	0.0213	0.9726	0.9801	
6		6	Noise-free	0.0203	0.9732	0.9817	
			Var=0.01	0.0213	0.9722	0.9798	
6		7	Noise-free	0.0204	0.9738	0.9819	
			Var=0.01	0.0214	0.9799	0.9799	
7		5	Noise-free	0.0203	0.9730	0.9815	
			Var=0.01	0.0213	0.9720	0.9796	
7		7	Noise-free	0.0206	0.9738	0.9813	
			Var=0.01	0.0216	0.9727	0.9791	
OurMethod		5	6	Noise-free	0.0044	0.9962	0.9944
				Var=0.01	0.0044	0.9962	0.9944
	5	7	Noise-free	0.0044	0.9959	0.9931	
			Var=0.01	0.0044	0.9959	0.9931	
	6	6	Noise-free	0.0044	0.9960	0.9934	
			Var=0.01	0.0044	0.9960	0.9934	
	6	7	Noise-free	0.0046	0.9954	0.9915	
			Var=0.01	0.0046	0.9954	0.9915	
	7	5	Noise-free	0.0044	0.9959	0.9934	
			Var=0.01	0.0044	0.9959	0.9934	
	7	7	Noise-free	0.0050	0.9947	0.9895	
			Var=0.01	0.0050	0.9947	0.9895	

MaxEntD leaves a lot of random noise at the peak position. Simultaneously, as can be seen in Table II, it is clear that our method exhibits excellent performance in the case of mixed convolution kernels in various situation. At the same time, our method has the same index result for noisy degraded

spectrum and no noisy degraded spectrum. However, it does not mean that the restored spectra in these two cases are exactly identical. They are different in some small detail areas.

TABLE III
COMPARISON OF POSITION AND INTENSITY FOR PEAK DISTORTIONS IN
FIG. 8 ($\rho_{gau} = 8, var = 10$).

Peak positions	Method	A(305)	B(372)	C(392)	RMSE
<i>Position</i> ¹	SBD-MHS	-1	-1	+1	1
	MaxEntD	-4	-1	+1	2.4504
	DSPNet	-7	-1	+2	4.2426
	OurMethod	-1	-2	+2	1.2901
<i>Intensity</i> ²	SBD-MHS	+0.0452	-0.0649	0.1028	0.0749
	MaxEntD	+0.0501	+0.0053	+0.0100	0.0297
	DSPNet	-0.0577	-0.0593	-0.0649	0.0375
	OurMethod	+0.0177	-0.0071	+0.0243	0.0140

¹ In cm^{-1} , obtained from the band maximum.

² "+" or "-" indicates larger or smaller than the original, respectively.

In order to further prove the superiority of our method in deconvolution problem. Experiments about the position and intensity of the peaks and valleys are designed. Table III and Fig.8 represent the peak distortion from the perspective of vision and data. The values of intensity and position for three peaks (A, B and C) are noted. It can be seen from the Table III that our approach has a lower RMSE for position and intensity. Thus, according to the above experiments, our method is robust and can be applied to various complex situations.

E. Real Spectrum Experiment

In the final stage of this work, real spectrum experiments are conducted to test the effectiveness of the proposed method. These real spectra are obtained from an aged Fourier transform infrared spectrometer.

1) *Real Degraded Spectrum*: These two spectra are good materials for testing the performances of our method. In Fig. 9 (a), the marked part of the spectrum is too smooth and the peaks seem to have been hidden seriously. It is extremely possible to find peaks here. Additionally, in Fig. 9 (c), there are two obvious overlaps in the spectrum which is marked.

2) *Real Spectrum Results*: As can be seen in Fig. 9 (b), there are three hidden peaks are found by our method, and the split peaks are marked with a star. In Fig. 9 (d), the original shallow peak is deeper now, and the overlap is split well. The split peaks are beneficial to indicate the property of the spectrum. However, there are still some problems, such as artificial noise and remaining overlap. Our method does not get a good grade in the part to be split in Fig. 9 (b). There is artificial noise in the reconstructed spectra which is marked with a square. In a word, our method could detect most overlap in real spectrum. Our method has a competitive performance compared with traditional approaches.

F. Limitations

Although our network has a great improvement in training and testing results compared with other methods, there is still a phenomenon that the deconvolution result is too high

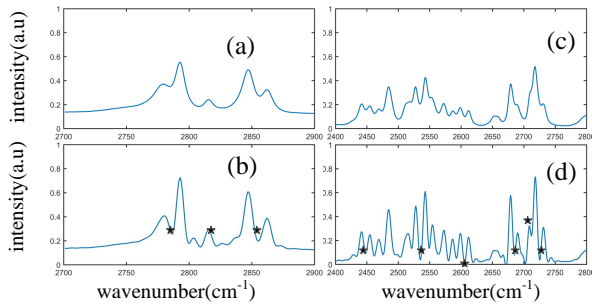


Fig. 9. Real Raman spectrum experiments. (a) Part of spectrum L(+)-Arabinofuranose from 2700 to 2900 cm^{-1} (b) Result of our method. (c) Part of spectrum D(-)-Ribose from 2400 to 2800 cm^{-1} (d) Result of our method.

or too low sometimes for the real degraded spectrum. The deconvolution results of complex wave can not be completely restored. Owing to the limitations, future work will focus on dealing with complex waves to make the network more general.

V. CONCLUSION

In this article, a new dual stream deconvolution spectrum analysis network is proposed. By strengthening the ability to express spectral characteristics, it greatly retains the high and low frequency information of the spectrum with strong anti-interference ability. A novel activation function is proposed to achieve the architecture of dual stream network. This activation function can let the hidden neural nodes receive the opposite input and weight. Regarding sample utilization, the proposed heuristic learning strategy uses self-defined schedule learning to solve the difficult problems of high sample repeatability. Through different comparative experiments, our model can also achieve good results compared with the latest methods. In the future, the disadvantages of the network and application of various fields will be focused.

REFERENCES

- [1] P. L. Silvestrelli, M. Bernasconi, and M. Parrinello, "Ab initio infrared spectrum of liquid water," *Chemical Physics Letters*, vol. 277, no. 5, pp. 478–482, 1997.
- [2] A. Patzer, M. Schütz, T. Möller, and O. Dopfer, "Infrared spectrum and structure of the adamantane cation: Direct evidence for jahn–teller distortion," *Angewandte Chemie International Edition*, vol. 51, no. 20, pp. 4925–4929, 2012.
- [3] M. J. Baker, J. Trevisan, P. Bassan, R. Bhargava, H. J. Butler, K. M. Dorling, P. R. Fielden, S. W. Fogarty, N. J. Fullwood, K. A. Heys, C. Hughes, P. Lasch, P. L. Martin-Hirsch, B. Obinaju, G. D. Sockalingum, J. Sulé-Suso, R. J. Strong, M. J. Walsh, B. R. Wood, and F. L. Martin, "Using fourier transform ir spectroscopy to analyze biological materials," *Nature Protocols*, vol. 9, no. 8, pp. 1771–1791, August 2014.
- [4] C. Hildebrandt, C. Raschner, and K. Ammer, "An overview of recent application of medical infrared thermography in sports medicine in austria," *Sensors*, vol. 10, no. 5, pp. 4700–4715, 2010.
- [5] J. Chen, D. Chen, X. Li, and K. Zhang, "Towards improving social communication skills with multimodal sensory information," *IEEE Transactions on Industrial Informatics*, vol. 10, no. 1, pp. 323–330, Feb 2014.
- [6] H. Baltacıoğlu, A. Bayındırlı, M. Severcan, and F. Severcan, "Effect of thermal treatment on secondary structure and conformational change of mushroom polyphenol oxidase (ppo) as food quality related enzyme: A ftir study," *Food Chemistry*, vol. 187, pp. 263–269, 2015.
- [7] J. K. Kauppinen, D. J. Moffatt, H. H. Mantsch, and D. G. Cameron, "Fourier transforms in the computation of self-deconvoluted and first-order derivative spectra of overlapped band contours," *Analytical Chemistry*, vol. 53, no. 9, pp. 1454–1457, 1981.
- [8] V. A. Lórenz-Fonfría and E. Padrós, "Maximum entropy deconvolution of infrared spectra: Use of a novel entropy expression without sign restriction," *Appl. Spectrosc.*, vol. 59, no. 4, pp. 474–486, Apr 2005.
- [9] L. Yan, H. Liu, S. Zhong, and H. Fang, "Semi-blind spectral deconvolution with adaptive tikhonov regularization," *Appl. Spectrosc.*, vol. 66, no. 11, pp. 1334–1346, Nov 2012.
- [10] L. Yan, H. Liu, L. Chen, H. Fang, Y. Chang, and T. Zhang, "Parametric semi-blind deconvolution algorithm with huber–markov regularization for passive millimeter-wave images," *Journal of Modern Optics*, vol. 60, no. 12, pp. 970–982, 2013.
- [11] H. Zhu and L. Deng, "Spectral restoration using semi-blind deconvolution method with detail-preserving regularization," *Infrared Physics and Technology*, vol. 69, pp. 206–210, 2015.
- [12] Y. Senga, K. Minami, S. Kawata, and S. Minami, "Estimation of spectral slit width and blind deconvolution of spectroscopic data by homomorphic filtering," *Appl. Opt.*, vol. 23, no. 10, pp. 1601–1608, May 1984.
- [13] S. Sarkar, P. K. Dutta, and N. C. Roy, "A blind-deconvolution approach for chromatographic and spectroscopic peak restoration," *IEEE Transactions on Instrumentation and Measurement*, vol. 47, no. 4, pp. 941–947, Aug 1998.
- [14] Z. Mou-Yan and R. Unbehauen, "A deconvolution method for spectroscopy," *Measurement Science and Technology*, vol. 6, no. 5, p. 482, 1995.
- [15] H. Liu, S. Liu, T. Huang, Z. Zhang, Y. Hu, and T. Zhang, "Infrared spectrum blind deconvolution algorithm via learned dictionaries and sparse representation," *Appl. Opt.*, vol. 55, no. 10, pp. 2813–2818, Apr 2016.
- [16] H. Su, F. Xing, X. Kong, Y. Xie, S. Zhang, and L. Yang, "Robust cell detection and segmentation in histopathological images using sparse reconstruction and stacked denoising autoencoders," in *Medical Image Computing and Computer-Assisted Intervention – MICCAI 2015*, N. Navab, J. Hornegger, W. M. Wells, and A. F. Frangi, Eds. Cham: Springer International Publishing, 2015, pp. 383–390.
- [17] S. Lefkimiatis, "Non-local color image denoising with convolutional neural networks," in *The IEEE Conference on Computer Vision and Pattern Recognition (CVPR)*, July 2017.
- [18] J. Zhang, J. Pan, W.-S. Lai, R. W. H. Lau, and M.-H. Yang, "Learning fully convolutional networks for iterative non-blind deconvolution," in *The IEEE Conference on Computer Vision and Pattern Recognition (CVPR)*, July 2017.
- [19] T.-Y. Lin, P. Dollar, R. Girshick, K. He, B. Hariharan, and S. Belongie, "Feature pyramid networks for object detection," in *The IEEE Conference on Computer Vision and Pattern Recognition (CVPR)*, July 2017.
- [20] H. Zhu, Y. Qiao, G. Xu, L. Deng, and Y. Yu-Feng, "Dspnet: A lightweight dilated convolution neural networks for spectral deconvolution with self-paced learning," *IEEE Transactions on Industrial Informatics*, pp. 1–1, 2019.
- [21] L. Jiang, D. Meng, S.-I. Yu, Z. Lan, S. Shan, and A. Hauptmann, "Self-paced learning with diversity," in *Advances in Neural Information Processing Systems 27*, Z. Ghahramani, M. Welling, C. Cortes, N. D. Lawrence, and K. Q. Weinberger, Eds. Curran Associates, Inc., 2014, pp. 2078–2086.
- [22] K. Ghasedi, X. Wang, C. Deng, and H. Huang, "Balanced self-paced learning for generative adversarial clustering network," in *The IEEE Conference on Computer Vision and Pattern Recognition (CVPR)*, June 2019.
- [23] T.-Y. Lin, A. RoyChowdhury, and S. Maji, "Bilinear cnn models for fine-grained visual recognition," in *The IEEE International Conference on Computer Vision (ICCV)*, December 2015.
- [24] K. Sun, J. Zhang, C. Zhang, and J. Hu, "Generalized extreme learning machine autoencoder and a new deep neural network," *Neurocomputing*, vol. 230, pp. 374–381, 2017.
- [25] H. Zhu, L. Deng, G. Xu, Y. Chen, and Y. Li, "Spectral semi-blind deconvolution methods based on modified ϕ s regularizations," *Optics & Laser Technology*, p. S0030399217312367, 2018.
- [26] H. Zhu, L. Deng, H. Li, and Y. Li, "Deconvolution methods based on convex regularization for spectral resolution enhancement," *Computers and Electrical Engineering*, vol. 70, pp. 959–967, 2018.



Lizhen Deng (M'17) received the B.S. degree in electronic information science and technology from Huaibei Coal Industry Teachers College, Huaibei, China, in 2007, and the M.S. degree in communication and information systems from Nanjing University of Aeronautics and Astronautics, Nanjing, China, in 2010. She received her Ph.D. degree in electrical engineering from Huazhong University of Science and Technology, China, in 2014. In 2014, she joined the Nanjing University of Posts and Telecommunications, Nanjing, China. Her current

research interests include image processing, computer vision, pattern recognition, and spectral data processing. E-mail: alicedenglzh@gmail.com



Guoxia Xu (M'19) received the B.S. degree in information and computer science from Yancheng Teachers University, Jiangsu Yancheng, China in 2015, and the M.S. degree in computer science and technology from Hohai University, Nanjing, China in 2018. He was a research assistant in City University of Hong Kong and Chinese University of Hong Kong. Now, he is pursuing his Ph.D. degree in Department of Computer Science, Norwegian University of Science and Technology, Gjøvik Norway. His research interest includes pattern recognition,

image processing, and computer vision. E-mail: gxXu.re@gmail.com



Yanyu Dai received B.S. degree in communication engineering from Jiangxi Normal University, Nanchang China, in 2018. He is now pursuing his master degree in electronic and communication engineering in Nanjing University of Posts and Telecommunications. His current research interest is deep learning. Email: 17805106175@163.com



Hu Zhu (M'17) received the B.S. degree in mathematics and applied mathematics from Huaibei Coal Industry Teachers College, Huaibei, China, in 2007, and the M.S. and Ph.D. degrees in computational mathematics and pattern recognition and intelligent systems from Huazhong University of Science and Technology, Wuhan, China, in 2009 and 2013, respectively. In 2013, he joined the Nanjing University of Posts and Telecommunications, Nanjing, China. His research interests include pattern recognition, image processing, and computer vision. E-mail: peter.hu.zhu@gmail.com

ter.hu.zhu@gmail.com